Robust Virtual Sensing for Vehicle Agile Manoeuvring: A Tyre-model-less Approach

Acosta, M, Kanarachos, S & Fitzpatrick, M

Original citation & hyperlink:
Acosta, M, Kanarachos, S & Fitzpatrick, M 2017, 'Robust Virtual Sensing for Vehicle Agile Manoeuvring: A Tyre-model-less Approach' *IEEE Transactions on Vehicular Technology*, vol (in press), pp. (in press)
https://dx.doi.org/10.1109/TVT.2017.2767942

DOI 10.1109/TVT.2017.2767942
ISSN 0018-9545
ESSN 1939-9359

Publisher: IEEE

Robust Virtual Sensing for Vehicle Agile Manoeuvring: A Tyre-model-less Approach.

Manuel Acosta, Stratis Kanarachos, and Michael E. Fitzpatrick

***Abstract*—This paper presents a robust virtual sensor to estimate the chassis planar motion states and the tyre forces during agile manoeuvres using a tyre-model-less approach. Specifically, virtual sensing is achieved from standard sensor signals available on the CAN bus of modern vehicles using a modular filter architecture composed of Stochastic Kalman Filters. A high-fidelity virtual testing environment is constructed in *IPG CarMaker*® using a driver-in-the-loop setup to verify the virtual sensor without compromising driver's safety. Moreover, road random profiles are incorporated into the virtual road to assess the state estimator robustness to high vertical excitation levels. The virtual sensor is simulated under drifting manoeuvres performed by an experienced test driver and tested experimentally under Fishhook and Slalom manoeuvres. Finally, the state estimator is integrated into a drift controller and autonomous drift control using exclusively readily available measurements is verified for the first time. As the drift equilibrium depends strongly on the tyre-road friction, an Adaptive Neuro-Fuzzy Inference System has been integrated into the virtual sensor structure to provide a continuous approximation of the road friction characteristics (axle lateral force versus slip curve) in rigid and loose surfaces. The findings suggest that it may be possible to develop advanced vehicle controllers without using a tyre model. This can lead to a substantial acceleration of development time, particularly in off-road applications, and remove the need for online estimation of tyre properties due to pressure, wear and age.**

***Keywords*—Virtual Sensing, Vehicle Agile Manoeuvring, Adaptive Neuro-Fuzzy Inference System, Autonomous Vehicle Control**

I. Introduction

In the near future, it is envisaged that autonomous vehicles will be able to operate efficiently at the limits of adhesion to exploit the full chassis potential. According to recent research, Modern Automotive Control Systems may be required to perform aggressive manoeuvres such as active drifting to maximise the lateral dynamics [1], [2] or vehicle posture control to reduce the severity of T-bone collisions [3]. In order to achieve such requirements an accurate and timely representation of the tyre forces and the vehicle planar velocities is necessary (e.g. body slip angle during active drift control). In addition, the operation of these systems should be robust against road friction uncertainties, and suitable for off-road applications where agile manoeuvring can be particularly beneficial [4].

Direct measurement of the forces generated by the tyres has been pursued in the literature employing load-sensing hub bearings [5] and strain-based measurements on the tyre [6] and the rim [7]. Nevertheless, this technology is still too complex and expensive to apply [8]. Concerning the measurement of the vehicle motion states, recent research has been proposed on Digital Image Correlation (DIC) [9] employing forward-facing mono and stereo cameras. Other methodologies based on Global Positioning System (GPS) signals and sensor fusion [10] have been suggested for this purpose, but issues such as intermittent visibility might limit the robustness of these approaches. For these reasons, virtual sensing based on readily-available measurements is still the preferred solution in the literature due to its cost-effectiveness and implementation simplicity [11], [12], [13], [14], [15].

Among the virtual sensing approaches proposed in the literature, Kalman Filtering techniques are most popular and have been used extensively in vehicle dynamics applications [13]. Unscented Kalman Filter (UKF) [14] and Extended Kalman Filter (EKF) [13] have been employed to handle the nonlinear vehicle planar dynamics. Depending on the architecture of the state estimator and the *a priori* knowledge of the road friction characteristics required to make the state estimator perform, tyre model-based [14], [13] and tyre model-less [12], [15] approaches can be distinguished. The former rely on a semi-empirical or semi-analytical tyre model (e.g. *Magic Formula* [14], *Dugoff* [13]) to approximate the road friction characteristics, while the latter assume that the friction forces are generated as a consequence of a stochastic process.

Apart from the considerable effort and resources needed to parameterize a tyre model [16], the major drawback of tyre model-based approaches is the lack of robustness against uncertain friction characteristics. While previous works have been proposed based on a continuous estimation of the road grip potential [14] and the subsequent adaptation of the tyre model using a grip scaling approach [17], these methodologies might fail to approximate loose surfaces such as deep snow or gravel. In these surfaces, the shape of the force versus tyre slip curve changes drastically [4] and a completely new parameterization may be necessary to capture the tyre behaviour [18].

Conversely, tyre-model-less approaches do not require any fixed tyre modelisation, which makes them especially suited for off-road applications or aggressive manoeuvring during which the tyre slips may leave the limits imposed by the tyre model parameterization and uncertainties in the tyre model dominate the response [19]. The traditional stochastic approach found in the literature consists of assuming that the tyre force generation mechanisms follow a random process, and the tyre forces are modelled as random-walk variables [11], [15], [20], [21], [22], [12], [23], [24], [25]. Specifically,

The authors are with the School of Mechanical, Aerospace and Automotive Engineering, Coventry University, Coventry, United Kingdom, e-mail: ac3354@coventry.ac.uk

in [11] the axle lateral forces are obtained from a random-walk UKF and the individual longitudinal forces are estimated using a Proportional-Integral-Derivative (PID) wheel rotating dynamics-based observer. These forces are used in a *Lugre* tyre model formulation to obtain the vehicle planar velocities. In [15], an EKF is employed to estimate at the same time the individual tyre lateral forces and the vehicle planar motion states. A similar approach was employed in [23], but axle lateral forces were calculated instead of individual forces. In [20], a single track model is employed, and the axle longitudinal forces are calculated from the wheel rotating dynamics in an EKF. A similar estimation structure was proposed in [21], and extended in [22] to handle individual longitudinal forces. In [24] the stochasticity of the tyre planar forces is evaluated and different autoregressive (AR) and autoregressive exogenous (ARX) models are proposed. In [12] a combined tyre-force estimation method is presented to approximate the tyre forces during aggressive manoeuvres based on the same random-walk principle. Other tyre model-less approaches exploiting Sliding Mode Observation (SMO) have been proposed in [25]. A detailed discussion regarding tyre model-less approaches can be found in the review [8], prepared by the authors in previous research steps.

This paper presents a virtual sensor to achieve autonomous drift control using cost-effective measurements. The previous shortcomings are overcome using a robust tyre-model-less approach, where virtual sensing is achieved during drifting manoeuvres employing a modular architecture composed of stochastic Kalman Filters. As the drift stabilisation depends greatly on the surface considered, a friction characterisation module is incorporated into the virtual sensor. Specifically, an Adaptive Neuro-Fuzzy Inference System (ANFIS) is integrated into the state estimator and an adaptation algorithm is developed to provide a continuous estimate of the axle lateral force versus slip curve. As analytical tyre models are avoided, this approach is potentially robust during off-road driving on loose surfaces, where a road friction classification relying on a grip scaling approach [17] might fail due to the distortion of the force versus slip curve. Apart from that, the virtual sensor proposed in this work does not require the execution of any kind of additional manoeuvres [26] and can be adjusted to different vehicle configurations with minimum effort. The rest of the paper is organised as follows.

In Section II, the architecture of the virtual sensor is presented. The vehicle planar dynamics and longitudinal force estimation modules are described in the corresponding subsections. In addition, details regarding the friction characterization module and the ANFIS adaptation algorithm are provided. The implementation of the virtual sensor in *IPG-CarMaker®* is described in Section III. The proposed virtual sensor is compared to other existing observers (tyre data-based and tyre model-based) developed in previous works on loose surfaces and inclined roads in the first part of Section IV. Simulation results obtained during manual and automated drifting manoeuvres are presented in the second part of the section. The experimental validation of the virtual sensor on Slalom and Fishhook tests is presented in Section V. Finally, conclusions and further research steps are provided in Section VI.

II. Virtual Sensor Structure

The structure of the virtual sensor is depicted schematically in Fig. 1. A modular architecture composed of three principal blocks —vertical tyre force estimation, longitudinal tyre force estimation, vehicle planar dynamics estimation— is proposed. The longitudinal and vertical force blocks have been addressed in our previous works [27], and thus here are merely introduced. Overall, the function of the virtual sensor can be defined in the following manner.

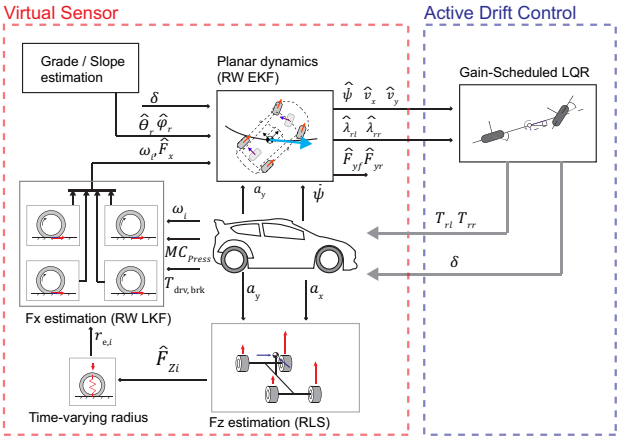

Fig. 1. Virtual sensor structure.

The vertical loads are estimated using Recursive Least Squares (RLS) and a quasi-static weight transfer model based on the roll stiffness distribution and the chassis geometric parameters [28]. These forces are used to calculate the effective radius (r_e) in a linear vertical stiffness model [27], [12]. The longitudinal forces are estimated using random-walk linear Kalman filters (RW-LKF) from wheel speed (ω), master cylinder pressure (MC_{press}), and driving-braking torque ($T_{drv,brk}$) measurements. A random-walk Extended Kalman Filter (RW-EKF) employs these forces in addition to the steering wheel angle (δ), wheel speed, and road inclination information ($\hat{\theta}_r, \hat{\phi}_r$) to estimate the axle lateral forces, road friction characteristics, vehicle planar motion states, and individual longitudinal slips. Further details regarding road inclination estimation can be found in [29]. Finally, the signals provided by the virtual sensor are used by a Gain-Scheduled Linear Quadratic Regulator (LQR) to determine the steering and rear torque inputs required to achieve the autonomous drift control task.

A. Vehicle Planar Dynamics Module

Following the scheme portrayed in Fig. 2, an upper-level (RW-EKF) provides continuous estimates of the axle lateral forces and vehicle planar motion states. Whilst these form part of the same state vector, two signals have been illustrated in Fig. 2 for better clarity. An ANFIS model is placed at a lower level to infer the tyre-road friction characteristics from the information provided by the RW-EKF. The uncertainty associated with the ANFIS model is quantified by means of the lateral force error ($\Delta\hat{F}_y$), which is smoothed using an RLS

block. When this error is above a certain threshold (i.e. ANFIS does not approximate well the real friction characteristics), the estimated axle lateral slips $\hat{\alpha}_i$ and axle lateral forces $\hat{F}_{yi}$ are stored progressively until a minimum amount of data is gathered, at which point the ANFIS learning process is triggered. This batch learning approach is run in parallel during the function of the virtual sensor and can be considered quasi-online learning due to the reduced time required to train the ANFIS structure ($t \approx 0.2s$, Table I). Additional details can be found in Section II-C.

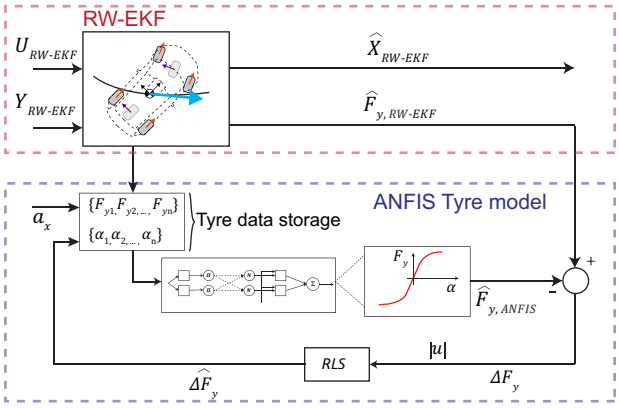

Fig. 2. Vehicle planar dynamics block: Random Walk EKF and ANFIS road characterisation modules.

1) Vehicle Modelling: A two-track vehicle model is used to capture the vehicle planar dynamics, equations (1-3). The vehicle mass is denoted by m, the yaw inertia by I_z, the distances from the front and rear axles to the centre of gravity by l_f and l_r respectively, and the angle steered by the front wheels by δ. The longitudinal and lateral velocities are v_x, v_y respectively, and $\dot{\psi}$ is the yaw rate. The road grade and road bank angle are referred as θ_r and ϕ_r respectively, and the front and rear track widths designated by tw_f,tw_r. The aerodynamic force is designated by F_{aero}, and is calculated as $0.5\rho A C_x v_x^2$, where ρ is the air density, C_x the drag coefficient, and A is a reference frontal area.

$$\begin{aligned} m(\dot{v}_x - \dot{\psi}v_y) &= (F_{x,fl} + F_{x,fr})\cos\delta - F_{y,f}\sin\delta \\ &+ F_{x,rl} + F_{x,rr} + mg\sin\theta_r - F_{aero} \end{aligned} \tag{1}$$

$$\begin{aligned} m(\dot{v}_y + \dot{\psi}v_x) &= (F_{x,fl} + F_{x,fr})\sin\delta + F_{y,f} \\ &+ F_{y,r} - mg\cos\theta_r \sin\phi_r \end{aligned} \tag{2}$$

$$\begin{aligned} I_z\ddot{\psi} &= ((F_{x,fl} + F_{x,fr})\sin\delta + F_{y,f})l_f \\ &- F_{y,r}l_r + \frac{tw_f}{2}(F_{x,fr} - F_{x,fl})\cos\delta \\ &+ \frac{tw_r}{2}(F_{x,rr} - F_{x,rl}) \end{aligned} \tag{3}$$

The individual lateral forces are lumped into axle lateral forces in order to make the system of equations solvable [11], [20], [12]. Thus, additional yaw moment terms derived from the longitudinal components of the individual lateral forces are neglected. The axle lateral slips (α_f, α_r) are computed from expressions (4-5).

$$\alpha_f = \delta - \arctan\left(\frac{\dot{\psi}l_f + v_y}{v_x}\right) \tag{4}$$

$$\alpha_r = -\arctan\left(\frac{-\dot{\psi}l_r + v_y}{v_x}\right) \tag{5}$$

Finally, the individual longitudinal slips (λ) are computed adopting the ISO convention, expression (6),

$$\lambda_{i,j} = \frac{\omega_{i,j} r_{e_{i,j}} - (v_x \pm \dot{\psi}\frac{tw_i}{2})}{v_x \pm \dot{\psi}\frac{tw_i}{2}} \tag{6}$$

where $w_{i,j}$ and $r_{e_{i,j}}$ are the wheel speed and effective radius respectively, with $i \in \{f, r\}$ (front, rear) and $j \in \{l, r\}$ (left, right).

2) Derivation of the Extended Kalman Filter: The vehicle dynamics equations (1-3) are discretized using a First order approximation ($e^{AT_s} \approx 1 + AT_s$), and presented as a general nonlinear discrete system of the form:

$$X_{k+1} = f(X_k, U_k) + w_k, \quad Y_{k+1} \quad = h(X_{k+1}, U_k) + v_k \tag{7}$$

Where $f(\cdot)$ and $h(\cdot)$ denote the state evolution and observation vectors, X_k is the vector of states, Y_{k+1} is the vector of measurements, and U_k the vector of inputs. w_k and v_k are the process uncertainty and measurement noise respectively, which are assumed to be Gaussian, uncorrelated and zero mean ($w_k \approx N(0, Q_k), v_k \approx N(0, R_k)$) [13]. According to [13], the filter function can be summarized by expressions (8-12).

$$\hat{X}_{k+1|k} = f(\hat{X}_{k|k}, U_k) \tag{8}$$

$$P_{k+1|k} = A_k P_{k|k} A_k^T + Q_k \tag{9}$$

$$K_k = P_{k+1|k} H_k^T [H_k P_{k+1|k} H_k^T + R_k]^{-1} \tag{10}$$

$$\hat{X}_{k+1|k+1} = \hat{X}_{k+1|k} + K_k[Y_k - h(\hat{X}_{k+1|k})] \tag{11}$$

$$P_{k+1|k+1} = [I - K_k H_k] P_{k+1|k} \tag{12}$$

During the *Time update* stage (8-9), the system states are calculated using the plant model. The predicted covariance matrix $P_{k+1|k}$ is calculated using the process covariance matrix Q_k and the Jacobian matrix A_k. In the *measurement update* stage (10-12), the system states are corrected with the measured quantities using the filter gain K_k and the system covariance matrix of the next step is computed $P_{k+1|k+1}$. The local observability of a nonlinear system has been addressed in the literature employing the Lie Derivative [13], [26] and by means of algebraic analysis of the observability matrix $O = [H, HA, HA^2, ..., HA^{n-1}]^T$, which is constructed from the linearised state-space model [20].

3) Stochastic Extended Kalman Filter (RW-EKF): The input, measurement, and state vectors of the RW-EKF are presented below for clarity (13-15).

$$X_{RW-EKF} = \{\hat{\dot{\psi}}, \hat{v}_x, \hat{v}_y, \hat{F}_{yf,RW}, \hat{F}_{yr,RW}\} \tag{13}$$

$$Y_{RW-EKF} = \{\dot{\psi}, v_x, a_{yc}, v_y^*\} \tag{14}$$

$$U_{RW-EKF} = \{\delta, \hat{F}_{x,i\in\{fl,fr,rl,rr\}}, \hat{\theta}_r, \hat{\phi}_r\} \tag{15}$$

The vector of states (X_{RW-EKF}) contains the yaw rate, longitudinal and lateral velocities, and axle lateral forces. The axle lateral forces are modelled using an auto-regressive model (AR) of the form $F_{y,k+1} = a_1 F_{y,k} + \Gamma_k$ [24]. The term Γ_k represents the random noise that drives the axle lateral forces, and a_1 is the AR regression factor, which was set to unity for simplicity. Other coefficients extracted from [24] were tested and negligible improvement was obtained. The vector of measurements (Y_{RW-EKF}) is made of the yaw rate, longitudinal velocity, compensated lateral acceleration (a_{yc}), and a pseudo-measurement of the lateral velocity (v_y^*). The compensated lateral acceleration is calculated from the measured lateral acceleration using the expression (16).

$$a_{y,c} = a_{y,m} - g\cos(\theta)\sin(\phi) + g\cos(\theta_r)\sin(\phi_r) \quad (16)$$

The term g is the gravity constant and θ, ϕ are the pitch and roll orientation angles of the vehicle with respect to an inertial reference frame. Details regarding the calculation of the chassis orientation angles can be found in our previous works [29]. The modular architecture proposed in this work facilitates the integration of an external road inclination observer [29].

The longitudinal velocity is calculated from the angular speed of the non-driven wheels, thus avoiding the use of GPS signals. If a front-wheel-drive (FWD) vehicle is considered, a reasonable assumption is to take the velocity of the wheel with the highest normal load as most representative of the "true" vehicle longitudinal velocity, calculated as $v_x = r_e\omega_{F_{z,max}} \pm \dot{\psi}\frac{tw_r}{2}$, where $\omega_{F_{z,max}}$ is the speed of the most loaded wheel. As this paper is focused on drifting manoeuvres, an additional approach to calculate the vehicle speed in a rear-wheel-drive (RWD) vehicle needs to be introduced. In this case, the angular speeds of the front non-driven wheels are considered. If a negligible longitudinal slip is assumed at the front wheels, the longitudinal velocity at the centre of gravity can be computed from the $j-th$ angular wheel speed using the expression (17).

$$v_x = \omega_{f,j} r_{e_{f,j}}(\cos(\delta) + \tan(\alpha_f)\sin(\delta)) \pm \dot{\psi}\frac{tw_f}{2} \quad (17)$$

With $j \in \{l, r\}$. In this equation α_f is the front axle lateral slip given by equation (4). Its value depends on other non-measurable motion states (such as the lateral velocity), and thus it is necessary to integrate expression (17) into the measurement vector of the filter. As the equation changes depending on the wheel considered ($\pm\dot{\psi}\frac{tw_f}{2}$ term) a hybrid modelisation would be necessary to implement expression (17). In order to avoid this, the average front wheel speed is taken and the yaw rate term is eliminated, obtaining expression (18). More complicated driveline architectures (all-wheel-drive) will be investigated in the future.

$$v_x = \left(\frac{\omega_{fl} r_{e,fl} + \omega_{fr} r_{e,fr}}{2}\right)(\cos(\delta) + \tan(\alpha_f)\sin(\delta)) \quad (18)$$

As the previous approaches might fail during non-constant speed events (e.g. severe wheel-lock during hard braking), it is necessary to introduce a covariance-scheduled strategy to make the filter perform in spite of plant systematic errors, selecting at each moment the most suitable measurement covariance (R_{RW-EKF}) values for each driving condition [30]. Two situations are considered depending on the master cylinder pressure (MC_{press}): braking situation ($MC_{press} > 20$ bar) and driving or coast down events ($MC_{press} < 20$ bar). In the former, the measurement covariance term ($R_{RW-EKF}(2,2)$) is increased to augment the uncertainty of the wheel speed measurements. In the latter case, the previous term is reduced to give more importance to the speed values obtained from expression (18). The 20 bar threshold was set to apply the covariance-scheduling only when there is a certain braking demand.

A preliminary observability analysis was performed on the linearized state-space model using the measurement vector $Y = \{\dot{\psi}, v_x, a_{yc}\}$. Nevertheless, this structure is unobservable in the absence of lateral excitation. The solution presented in [20] to handle this issue is to switch off the observer whenever observability conditions are not met. This may lead to continuous chattering during motorway or on-centre driving, where the lateral acceleration rarely exceeds the $2m/s^2$ threshold. In order to avoid this, the authors suggest the use of a pseudo-measurement of the lateral velocity v_y^*. This approach has been employed in other filter architectures with great success [31]. Moreover, the proposed pseudo-measurement prevents large drifts on the estimated lateral velocity when driving on severely inclined roads, Section IV-A3. In this case, the lateral velocity is assumed to be zero ($v_y^* \approx 0$), and the measurement covariance term ($R_{RW-EKF}(4,4)$) associated with this signal is adjusted according to the driving situation. These situations are regular driving and agile manoeuvring. While the estimate of the body slip angle ($\arctan\frac{v_y}{v_x}$) at t_{k-1} remains below a certain threshold, the assumption of near zero lateral velocity is maintained, and the measurement covariance term is given a low value. On the other hand, when the body slip angle passes the latter threshold, the measurement covariance term is increased to reduce the confidence on the near-zero lateral velocity assumption. Accurate results were found in both regular manoeuvres (e.g. Slalom) and drifting manoeuvres with a body slip threshold of 5 degrees.

B. Longitudinal Force Module

The wheel rotating dynamics are modelled by expression (19).

$$I_w\dot{\omega} = T_{drv} - T_{brk} - F_z\eta r_e - F_x r_e \quad (19)$$

Where I_w is the rotating inertia seen at the wheel frame, T_{drv},T_{brk} are the driving and braking wheel torques, η is the rolling resistance factor and r_e is the effective radius. The driving torque can be obtained from the engine torque using the transmission ratios and the final drive ratio [27]. In the case of active or Limited Slip Differentials, additional considerations are required [1]. The braking torque is obtained from the master cylinder pressure and the brake bias distribution. For additional details [27], [32] can be consulted. The

longitudinal forces are modelled as random-walk variables, and the regression term a_1 introduced previously is set to unity for simplicity. Equation (19) is discretized and presented in state-space form, obtaining the following state X_{RW-LKF}, measurement Y_{RW-LKF}, and input U_{RW-LKF} vectors.

$$X_{RW-LKF} = \{\omega, F_x\} \tag{20}$$
$$Y_{RW-LKF} = \{\omega\} \tag{21}$$
$$U_{RW-LKF} = \{T_{drv}, T_{brk}, F_z\} \tag{22}$$

The state-space model is implemented in a Linear Kalman Filter (RW-LKF). Following a similar approach to the planar dynamics model, the process covariance matrix is adjusted to reduce the influence of the systematic errors present in the filter model. Two situations (steady-state and transient) are considered to set the process covariance matrix Q_{RW-LKF} depending on the transient content of the longitudinal dynamics. Each driving condition is identified by monitoring the rate of change of the brake, gas, and clutch pedals, Section III-A.

C. Road friction characterisation with ANFIS

As mentioned previously, the road friction characteristics, and in particular the axle lateral force versus lateral slip curves, are approximated by an ANFIS model. A deeper discussion regarding ANFIS theory is skipped here due to space limitations and can be found in [33]. The analysis presented here is focused on the applicability of ANFIS models to road friction characterisation. A Single-Input Single-Output (SISO) Sugeno-type Fuzzy Inference System is used in this paper to model the nonlinear lateral force function ($F_y = f(\alpha)$). The *anfis.m* routine is used in *Matlab*® to generate the Sugeno-Type structure. Initially, different numbers of membership functions (MF) were tested to determine the ANFIS structure that best fits a sample tyre data set. Specifically, structures composed of 2, 4 and 6 MFs were constructed following the input grid partition method and used to approximate the tyre data generated in a Slalom manoeuvre using a *MF6.1 Tyre model* [17] and an experimentally validated compact-class vehicle model [26] in *IPG-CarMaker*® Fig 3.

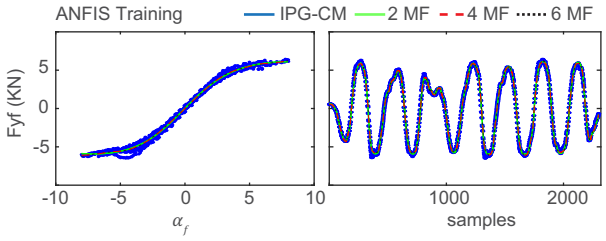

Fig. 3. ANFIS sensitivity analysis for different number of membership functions.

The maximum number of epochs was limited to 20 in order to reduce the training time. Higher numbers were tested and significant improvement was not obtained, Table I. As no significant differences were noticed between the performance of the three structures (2, 4, and 6 MFs), the structure with the minimum size was selected in order to reduce the training time.

TABLE I
ANFIS ERROR AND TRAINING TIME.

MF	$epochs$	$t\ (s)$	$e_f\ (N)$	$e_r\ (N)$
2	20	0.171	259.41	166.49
4	20	0.446	254.25	164.50
6	20	0.920	251.37	163.49
2	50	0.399	258.81	165.71
2	100	0.788	258.51	165.02

The training times for a sample of size 2301 are provided in Table I. As the training time for a maximum number of 20 epochs and 2 MFs is negligible ($\approx 0.2s$) the assumption of online ANFIS adaptation can be considered valid.

1) ANFIS adaptation algorithm: The adaptation process of the ANFIS model is presented schematically in Fig. 4. Continuous estimates of the axle lateral forces and axle lateral slips are provided at each time step by the vehicle planar dynamics state estimator (RW-EKF). The first block (*driving state*) is employed to "filter" the input data, passing data only during constant speed situations. This aims to eliminate non-representative samples of combined efforts (e.g. braking in a turn, power on) that would require the inclusion of additional inputs (longitudinal slip) in the ANFIS model. A second block (ANFIS uncertainty) is used to avoid unnecessary adaptation, thus limiting the number of training events to situations in which the ANFIS model presents a certain level of uncertainty. A bounded normalised factor ($\xi_k \in [0, 1]$) is employed to quantify the uncertainty associated with the ANFIS model. Low values indicate a good match between the ANFIS model and the real road-friction characteristics whereas values close to unity indicate a poor performance of the ANFIS model. This factor is determined with expressions (23-25).

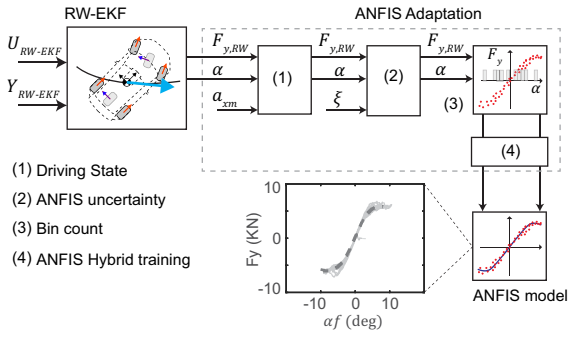

Fig. 4. ANFIS learning sequence.

$$\Delta F_{y,k} = |\hat{F}_{yf,RW_k} - \hat{F}_{yf,ANFIS_k}| + |\hat{F}_{yr,RW_k} - \hat{F}_{yr,ANFIS_k}| \tag{23}$$
$$\Delta \hat{F}_{y,k} = RLS(\Delta F_{y,k}) \tag{24}$$
$$\xi_k = \frac{\Delta \hat{F}_{y,k}}{C} \tag{25}$$

First, the axle lateral force error ($\Delta F_{y,k}$) is computed using expression (23). A Recursive Least Squares (RLS) block is employed to reduce the noise present in the signal and provide the most probable values of the noise-corrupted signal [26], [28], expression (24). An exponential factor λ_{ANFIS} is employed to reduce the relative importance of the old samples on the current prediction. Smaller values are used to reduce the importance of the previous samples and increase the adaptation rate [34]. Finally, the weighting factor ξ_k is obtained after normalizing the term $\Delta\hat{F}_{y,k}$ using equation (25). The term C is the maximum admissible error of the estimate $\Delta\hat{F}_{y,k}$, and was adjusted empirically. $\Delta\hat{F}_{y,k}$ is rectified with the term C before applying equation (25) to have a normalised weight factor bounded in the interval $[0, 1]$. Accurate results were obtained setting C to 1 KN and employing a forgetting factor $\lambda_{ANFIS} = 0.999$ in the RLS algorithm. When the level of uncertainty (ξ_k) is above a certain threshold (ξ_{thres}) the training samples are stored in a third block (*bin count*). A *bin count* approach is used in the last step in order to avoid overfitting in local regions and extrapolation issues derived from uneven sample concentrations. The axle lateral slip range is evenly distributed in n_{int} intervals, and the number of valid samples entering the block and remaining within each range (n_s) is counted. When an interval reaches a minimum number of samples n_{min} this is assigned a binary value $c_i = 1$. At each time step, the filling factor c_{fill} is computed from expression (26).

$$c_{fill} = \frac{\sum_{j=1}^{n_{int}} c_i}{n_{int}} \tag{26}$$

The training of the ANFIS network is triggered once the filling factor c_{fill} reaches a certain threshold (e.g. 50%), indicating that there are sufficient samples distributed along at least 50% of a predefined ANFIS input range (α_{lim}). Finally, the new samples are concatenated into the existing training dataset and the last V samples are employed to train the ANFIS model using a hybrid learning algorithm which combines the gradient method and the Least Squares Estimate (LSE) [33]. The elimination of older samples guarantees a quick adaptability of the model during mu-varying events. The parameters employed in this paper for the ANFIS adaptation are presented in Table II and were determined empirically after testing the ANFIS model in different mu-varying situations.

TABLE II
ANFIS ADAPTATION PARAMETERS

c_{fill} (%)	ξ_{thres}	n_{int}	α_{lim} (deg)	n_{min}	V
50	0.4	20	5	30	3000

III. VIRTUAL SENSOR IMPLEMENTATION

The virtual sensor is implemented in *IPG-CarMaker*® using the *CM4SL* library in *Matlab*®. A discretization time of $1ms$ is used to run the Kalman Filter equations and the simulation signals are acquired from the simulation model at 100 Hz using a zero-order hold. Coarser discretization times were not evaluated, as a real-time execution was achieved for $1ms$ in a computer equipped with an Intel(R)Core(TM) i7-3632QM CPU @ 2.2 GHz processor, 8GB RAM and 64-bit *Simulink*®. In order to evaluate the performance of the virtual sensor realistically, an additive noise model was employed to incorporate a random noise source on the measured signals [26]. The standard deviations of the noise sources were extracted from datasheets of state-of-the-art instrumentation [35].

A. Covariance-scheduling

The success of the covariance-scheduling approach is greatly affected by the ability of the virtual sensor to identify the current driving situation. In [36] a brief survey regarding pattern recognition approaches for automotive applications is provided. Relevant works exist to identify the *driving styles* [37], *driving skills* [38], or *car-following* behavior [39] employing Support Vector Machines (SVM), Neural Networks (NN), or Decision Tree (DT) among other methods. In this case, a DT algorithm is sufficient to achieve good results. Specifically, the transient content of the longitudinal dynamics is recognised by monitoring the total rate of change of the gas, clutch, and braking pedals. The Root Mean Square (RMS) value of this sum is used to adjust the process covariance matrix term of the driven wheels. In addition, the rate of change of the brake pedal is used to adjust the process covariance matrix term of the non-driven wheels during braking inputs.

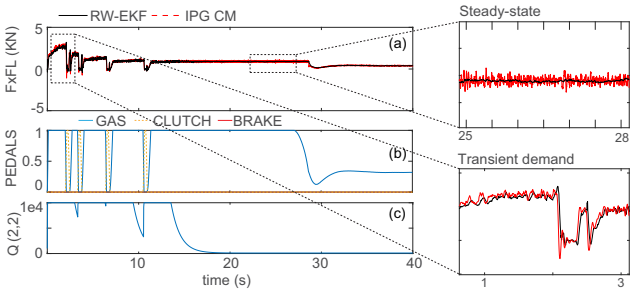

Fig. 5. Longitudinal force estimation in high-mu launch. (a) $F_{x,fl}$, (b) Position of the pedals, (c) Q_{RW-LKF}(2,2) term.

As can be noticed in Fig. 5, the term $Q_{RW-LKF}(2, 2)$ is increased during aggressive acceleration and gear shifting to improve the dynamic response of the random-walk longitudinal force. When the driver maintains the pedal position or moves it gently, the latter term is decreased to reduce the noise level in the estimated signal. As mentioned previously, the covariance values are determined using a decision tree based on $if - then$ rules. The transition between target values is modelled as a first-order response, Fig. 5, using the expression $Q_{k+1} = Q_k + T_s a_Q(-Q_k + Q_{ss,k})$, where the parameter a_Q is adjusted to add a certain degree of hysteresis and avoid excessive chattering. The stability of the state estimators for intermediate process covariance values was studied empirically and issues were not found. High values ($a_Q = 100$) were employed to achieve a quick convergence to the new references ($Q_{ss,k}$) when high process covariance values are required during high longitudinal demands. Low values ($a_Q = 1$) are employed to add additional hysteresis

and avoid chattering (e.g. during gear shifting). The same first-order strategy was implemented in the RW-EKF to adjust the term $R_{RW-EKF}(2,2)$ during braking events.

B. Virtual Testing Environment

1) Driving Simulator: A static force-feedback driver-in-the-loop (DIL) setup [40] was employed with the aim to evaluate the virtual sensor performance during extreme manoeuvres (e.g. *drifting*) without compromising driver's safety. The driver inputs (steering wheel angle, accelerator pedal, braking pedal, clutch pedal, and gear) are captured by the *Logitech®G-27* driving peripherals. These signals are then introduced in the *IPG-CarMaker®* model using the *CM4SL* library and the *Joystick* block of *Simulink®*. For additional details [40] can be consulted.

2) Road Profile Generation: In this paper, a random profile generation process based on the Sayers pseudo-random model [41] was followed to model the road irregularities and test the virtual sensor robustness to high vertical excitation levels. Additional details regarding the road profile generation are omitted due to space limitations and can be found on [40]. The road random profiles are generated numerically in *Matlab®* and implemented in *IPG-CarMaker®*. To validate the approach, different road categories were generated and their Power Spectral Densities (PSD) were compared to those recommended in ISO 8608:2016 [42]. Rough road profiles and smooth road profiles were employed for loose surfaces and asphalt tests respectively. A certain degree of correlation between the left- and right-hand profiles was assumed following the *shaping filter* approach presented in [41]. A separation of $1.5m$ was selected between both profiles following recommendations from [41]. The points lying between the two wheel-track lines are obtained by linear interpolation of the left- and right-handed wheel track profiles. For segments wider than $1.5m$ (e.g. dynamic platform), the same road patron is assumed and extended laterally. The *.crg* road property files needed to implement the road random profiles in *IPG-CarMaker®* were generated in *Matlab®* with the open source platform *openCRG.1.1.0*, [43].

IV. Simulation Results

A. Why this observer design?

This virtual sensor is the result of an iterative design process. In addition to the major requirement imposed to this work (i.e. design a virtual sensor suitable for aggressive agile manoeuvring), the observer should be able to overcome two critical limitations exhibited by previous works found in the literature: robustness to loose surfaces and robustness to road inclination angles. The final design should be able to perform accurately under agile manoeuvres (e.g. drifting) and, at the same time, fulfil the previous limitations to perform robustly during conventional manoeuvres in spite of the road surface or the road inclination.

1) Loose surfaces: In the first place, the proposed observer was compared to a data-based Extended Kalman Filter (NN-EKF) developed by the authors [26] and to a Magic Formula Extended Kalman Filter (MF-EKF). In the former approach, the tyre forces are approximated by a Neural Network (NN) structure. Moreover, the observer uses a road grip scaling approach to adjust the estimated tyre forces depending on the road grip potential $\mu_{\max}$ (assumed to lie between $\mu_{\max} = 0.2$ and $\mu_{\max} = 1$). For further details, [26] can be consulted. The NN structure was trained with data from an experimentally validated compact-class vehicle model equipped with a MF 6.1 tyre model (Size: $205 - 65/R16$) characterised on a rigid surface. The latter observer, MF-EKF, substitutes the NN with a simplified Magic Formula tyre model (Tyre-2, wet asphalt [4]) and assumes that the road grip potential is a known state, as in [13]. The longitudinal tyre forces required by the benchmarked observers were calculated with the RW-LKF estimation modules presented in Section II.

A first sinusoidal steering test was performed on a low mu rigid surface (wet asphalt, $\mu_{\max} = 0.6$), employing the parameters from a compact-class-like tyre model, denoted as Tyre-2 in [4]. As can be seen in Fig. 6-a, the proposed design (RW-EKF), the MF-EKF and the NN-EKF approximate very well the vehicle body slip and the axle lateral forces. Moreover, the NN-EKF is able to provide an online accurate estimation of the road grip potential, demonstrating the ability of this approach to estimate the maximum road friction ($\mu_{\max}$) of rigid surfaces.

The same sinusoidal test was repeated on a low mu loose surface (gravel, $\mu_{\max} = 0.6$), using the parameters corresponding to the tyre designated as Tyre-4, [4]. In order to establish a fair comparison, the tyre parameters employed in this analysis were determined using the same tyre characterised on different surfaces [4]. The parameters of the MF-EKF were kept unaltered, assuming that a Magic Formula grip scaling correction [17] of the true surface grip potential is employed on a tyre model parameterised by conventional means (i.e. on a rigid surface). As can be noticed in Fig. 6-b, the tyre model-based approaches (MF-EKF and NN-EKF) fail to predict the vehicle body slip and the axle lateral forces. In particular, the NN-EKF is unable to estimate accurately the surface grip potential and underestimates the vehicle body slip. This malfunction is caused by the extreme reduction of the cornering stiffness and the monotonic friction characteristics exhibited by loose surfaces, where the maximum friction depends on phenomena such as the *buldozzing* effect, and is generated at high wheel slip angles [18], [4]. The maximum body slip error of the MF-EKF and NN-EKF observers is close to 10 degrees, which limits the applicability of these tyre model-based approaches on extreme off-road surfaces. Overall, despite these results might vary in absolute terms in a real environment, the patterns exhibited by this analysis evidence that the use of a tyre model or a data-based structure characterised on rigid surfaces should be avoided when dealing with extreme off-road surfaces. In these conditions, a tyre model-less approach is preferred.

2) Yaw Stability Control (YSC): In order to assess the influence of the state estimator accuracy on the vehicle safety, the observers compared in the previous section (NN-EKF and RW-EKF) were implemented in a Yaw Stability Control (YSC) system [30]. The YSC design described in [30] introduces a differential braking action to maintain the vehicle yaw rate and body slip within the linear region limits [30]. The con-

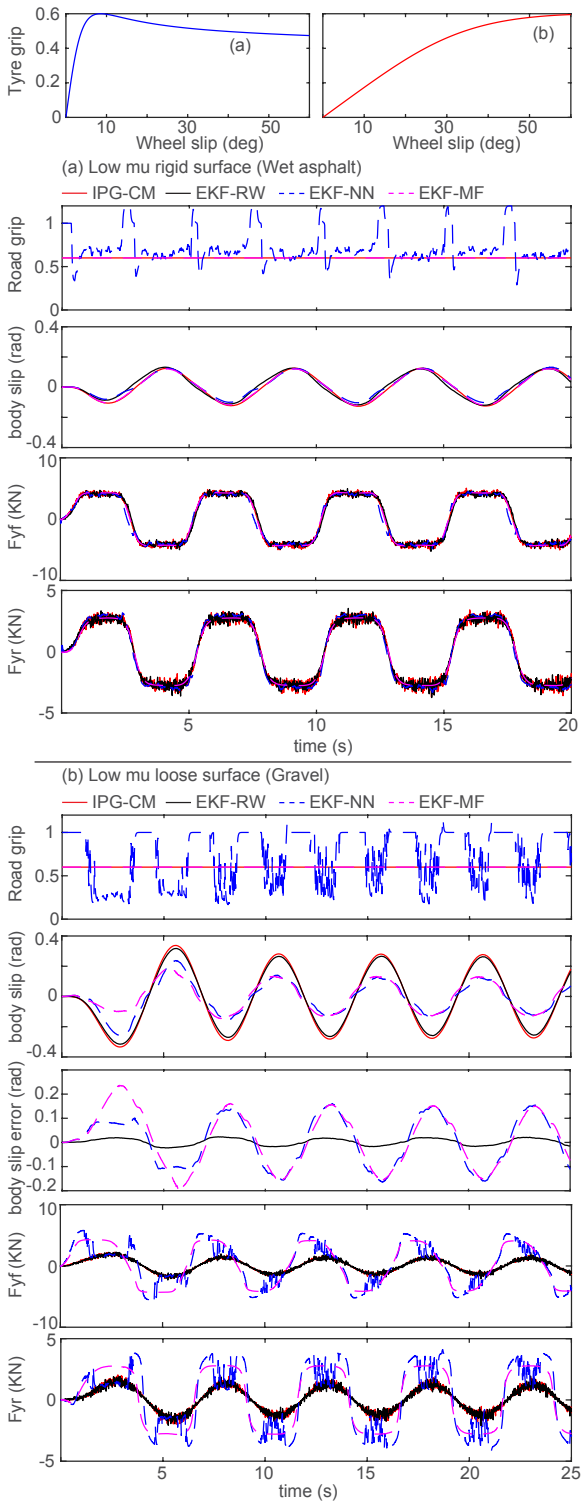

Fig. 6. Sinusoidal test, 80kph, 90 degrees input, Freq. 0.2 Hz. (a) Wet rigid surface (Tyre-2 [4]), (b) Gravel Loose surface (Tyre-4 [4]).

troller gain was obtained using a Linear Quadratic Regulator formulation. It must be remarked that the focus of this work lies in the development of the virtual sensor, and therefore the YSC is introduced here merely to study the influence of the observer accuracy on the vehicle stability. Sine with Dwell tests [26] were simulated on rigid (asphalt high mu, low mu), and loose surfaces (gravel). Usually, the YSC activation threshold depends on the road grip potential [44], [30]. In this study, a worst case scenario is considered (e.g. a quick transition from high to low mu), and the same yaw rate and body slip thresholds were used during the three simulations ($|\dot{\psi}_{max}| = \frac{8m/s^2}{v_x}$, $|\beta_{\max}| \approx 8deg$, [30]). The YSC equipped with the observers (RW-EKF and NN-EKF) restricted the vehicle response within the desired thresholds during the tests performed on rigid surfaces, Fig. 7. Severe vehicle instability (spin) was observed with the YSC disabled. A slight deviation is seen on the NN-EKF estimates due to the differential braking action of the YSC, which is not included on the virtual sensor model (Single-track modelisation). Additional results regarding the high-mu tests are omitted due to space limitations.

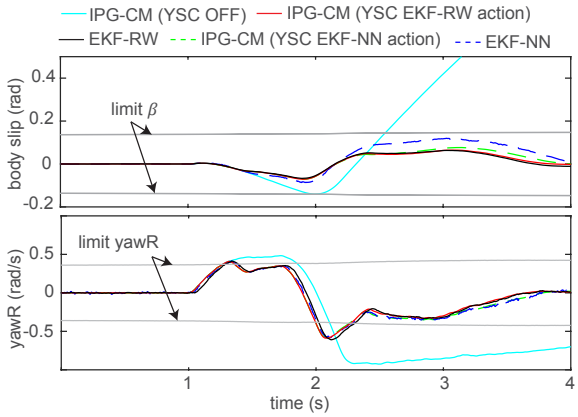

Fig. 7. Sine with Dwell test, 80 kph, Wet asphalt $\mu_{\max} = 0.6$, 160 degrees input. MF. 6.1 tyre model [26].

As can be seen in Fig. 8, the performance of the data-based observer (NN-EKF) was significantly worsened during the test executed on gravel (a large error is observed on the estimated vehicle body slip). This affects significantly the stability of the vehicle, as the YSC is not able to maintain the vehicle within the required body slip threshold and a maximum body slip angle $\beta \approx 20$ degrees is reached. On the other hand, the YSC equipped with the proposed observer (RW-EKF) was able to follow closely the maximum body slip thresholds. Once again, it is evidenced that a cautious treatment of loose surfaces is necessary when tyre model-based observers are employed. As the tyre model-based approaches did not guarantee the minimum stability requirements on loose surfaces, their design was not considered in further steps of this work, and therefore only tyre model-less approaches were studied after this point.

3) Inclined roads: In the introductory section different stochastic approaches were discussed. A common point shared by these works is that a detailed evaluation of the stochastic virtual sensors on inclined roads is missing. Initially, the proposed design was constructed using a reduced vector of measurements ($Y_{initial} = \{\dot{\psi}, v_x, a_{yc}\}$, inspired by previous designs found on the literature [20]. This design was tested driving aggressively on the Nordschleife virtual road of IPG-CarMaker (employing the DIL setup described in Section III-B1). The slope and bank angles were estimated by an

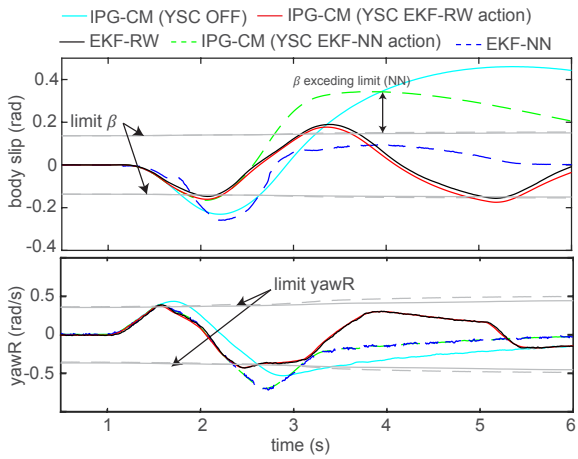

Fig. 8. Sine with Dwell test, 80 kph, 245 degrees input, Gravel terrain $\mu_{\max} = 0.6$. MF Isotropic Gravel tyre model [4].

external road characterisation block developed by the authors in previous research steps [29].

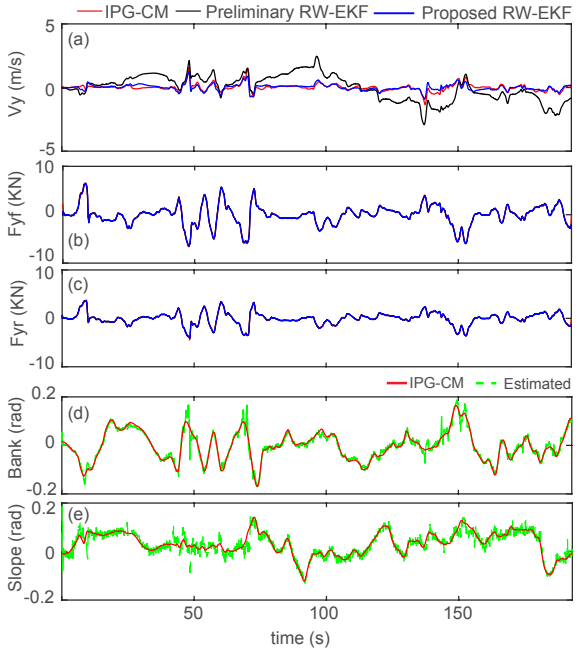

Fig. 9. Banked road test, Nordschleife. (a) Lateral velocity, (b) Front axle lateral force, (c) Rear axle lateral force, (d) Bank angle and (e) Slope angle.

As can be seen in Fig. 9, the preliminary design (with the vector of measurements $Y_{initial}$) exhibits large drifts on the lateral velocity during low lateral excitations (straight-line driving), caused by small biases on the compensated lateral acceleration (a_{yc}) derived from errors in the estimation of the road inclination. A pseudo-measurement of the lateral velocity (Section II-A3) was introduced in the proposed approach in order to overcome the lateral velocity drift seen during low lateral excitations on banked roads. This solution improved significantly the lateral velocity estimation accuracy (reducing the Normalised Root Mean Square Error NRMSE from 50% to approximately 10%). The proposed approach keeps the maximum body slip error on severe inclined roads below the two-degree band, which helps to prevent the YSC system from false interventions. Additional comparisons were not possible due to the lack of works testing stochastic observers on inclined roads. Nevertheless, results indicate that the proposed novel construction can handle better the lateral velocity drift derived from slight biases on the lateral acceleration measurements.

B. Drifting manoeuvres

The previous analyses evidenced the superior performance of the proposed approach for low body slip applications, particularly on loose surfaces. As the rest of virtual sensors discussed previously were unable to fulfil minimum performance requirements on these conditions, their study is omitted in this section.

TABLE III
CATALOG OF DRIFTING MANOEUVRES. OD: OPEN DIFFERENTIAL, EV: ELECTRIC VEHICLE

Test	Bodyslip (*deg*)	Grip	Configuration	Road
Manual Drifting Tests (Driver: C2 IDIADA Driving License)				
#1-*Drift R=20*	$30-40$	≈ 0.6	*OD-RWD*	Rough
#2-*Limit Drift*	$30-40$	≈ 0.6	*OD-RWD*	Rough
Autonomous Drift Controller				
#3-*R=10*	40	≈ 0.6	*EV-RWD*	Rough
#4-*Clothoid*	30	≈ 0.6	*EV-RWD*	Rough

1) Manual drifting tests: The virtual sensor was evaluated following the catalogue of manoeuvres presented in Table III. A compact-class RWD vehicle model equipped with an open differential was employed during the first part of the virtual sensor evaluation (tests $\#1-\#2$, which were carried out using the DIL setup described in Section III-B1). The vehicle model was created in *IPG-CarMaker®* taking as a reference the experimentally validated compact-class model used in previous works [26]. The gravel parameters introduced in the previous section and detailed in [4] (Tyre 4) were employed during the simulations. The ANFIS adaptation algorithm was disabled during these tests, and its analysis is covered under constant-speed manoeuvres in Section IV-C. A rough road profile was superimposed to the virtual road with the aim to increase the level of vertical excitation, as expected from loose surfaces. During the first test, the vehicle is driven and controlled around large body slip angles (30 to 40 degrees) following a 20-meter-radius circular path, Fig. 10. Overall, the motion states and forces estimated by the RW-EKF are very accurate. The vehicle turns counterclockwise, and the vertical load on the rear inner wheel (RL) is reduced due to the lateral weight transfer. As the vehicle is equipped with an open differential, the inner rear wheel receives greater power and increases its velocity considerably, Fig. 10. The estimates of the axle lateral forces present a high noise level due to the vertical excitation induced from the rough road profile.

In the second test, the vehicle was driven at the limits of handling along the gravel segment depicted in Fig. 11,

(test #2). The body slip angle is increased deliberately and maintained along the turns in order to maximise the lateral acceleration [1], [4], [2]. High yaw accelerations are generated to change the vehicle attitude fast and concatenate turns [2]. Overall, the vehicle planar velocities estimated by the RW-EKF follow closely the simulation signals, Fig. 12.

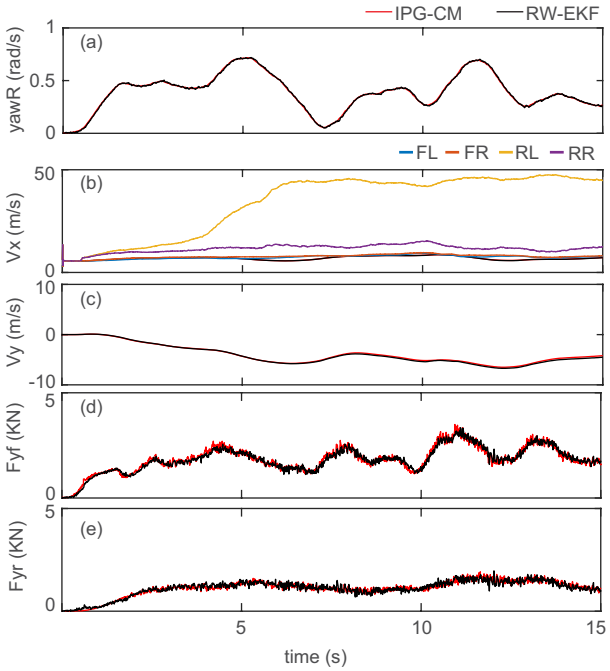

Fig. 10. Test (#1), Drifting on gravel $R = 20m$. (a) Yaw rate, (b) Longitudinal velocity, (c) lateral velocity, (d-e) Front-Rear axle lateral forces.

The longitudinal velocity is approximated with high accuracy in spite of the severe wheel-locks experienced at $t \approx 15s$ and $t \approx 90s$, demonstrating the suitability of the covariance-scheduled approach. Slight offsets are seen on the lateral velocity during time intervals 5-15s and 90-100s. Despite this, the NRMSE remains well below the 5% threshold for all the vehicle planar motion states, see Section IV-B3.

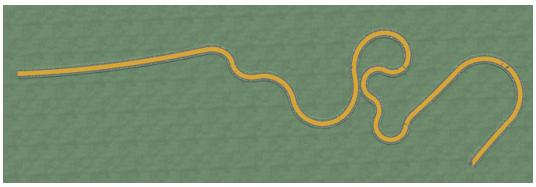

Fig. 11. Virtual Gravel road generated in *IPG-CarMaker*® by concatenation of arc and clothoid segments, test (#2).

The individual longitudinal forces are depicted in Fig. 13. In spite of the aggressiveness of the manoeuvres, the RW-LKF approximates very well the simulation signals.

2) Autonomous Drift Control (ADC): As the final goal of the virtual sensor is to provide the state feedback required to achieve drift control from readily-available measurements, additional simulations (tests $\#3-\#4$) were performed using a preliminary drift controller based on a gain-scheduled LQR architecture, Fig. 14. This controller provides the steering inputs and rear longitudinal slips ($U_{LQR} = \{\delta, \lambda_{RL}, \lambda_{RR}\}$) necessary to stabilize the vehicle around the drift equilibrium states (x_{ss}). The driving torques required to track the longitudinal slips imposed by the LQR are computed using a proportional-integral (PI) controller. A similar control architecture has been studied by the authors in previous works [2] assuming full state feedback available. In this section, this assumption is eliminated and the states obtained from the RW-EKF are employed in the controller, $X_{LQR} = \hat{X}_{RW-EKF}$. In order to ensure a real-time implementation, the gains of the LQR were computed offline for a set of equilibrium points and stored in look-up tables. At this point, it must be remarked that the focus of this work lies in the development of the virtual sensor. The refinement of the drift controller and its comparison to other control architectures (Model Predictive Control, MPC) is currently being investigated by the authors. First findings demonstrate the superior ability of the MPC to handle constraints on the maximum steering rate at the expense of higher computational resources, [45].

A reference sport-class vehicle model provided by the *IPG-Carmaker*® library was employed during the simulations. The PI controller was implemented using the user rear-wheel-drive powertrain model in *IPG-CarMaker*®. Individual torque action was implemented (i.e. in-wheel motors) and the maximum power and torque values were limited to $50KW$ and $800Nm$ respectively [46]. A complete evaluation of the drift controller using a more detailed model will be pursued in future research steps. The drift equilibrium solutions were computed offline following the procedure presented in [1], [2]. For simplicity, a lumped model was employed to obtain these solutions, and thus a unique rear longitudinal slip was considered for the rear wheels. More complex driveline setups can be found in [1], [45] and will be explored in the future. The clothoid test was carried out to demonstrate the suitability of the drift controller to follow paths of arbitrary road geometries, Fig. 15. The path following task is achieved incorporating an upper-level PID controller that adjusts the road curvature (κ) required by the drift equilibrium solutions to minimise the lateral deviation error (e_y), Fig. 14. A similar controller architecture can be consulted in [2]. The results of the clothoid-drift test ($\#4$) are depicted in Fig. 16. Some oscillations in the target signals are noticed due to the regulation action of the upper-level controller to minimise the lateral deviation error. Overall, the precision of the virtual sensor is remarkable. Similar performance levels were obtained on the constant-radius drift test ($\#3$), Table IV. Additional graphs are omitted due to space limitations.

3) Metrics: To conclude with this section, the precision of the virtual sensor is quantified numerically using the NRMSE, [13], [26]. The NRMSE corresponding to the vehicle motion states and the axle lateral forces are provided in Table IV.

Overall, all the errors lie well below the 10% threshold. Numerical errors from other works found in the literature range from 5 to 10%, [13], [32]. Nevertheless, in these works drifting manoeuvres were not considered, and thus a more detailed comparison can not be established. Moreover, additional hypotheses such as the availability of a tyre model embedded in the observer, *a priori* known road-friction characteristics,

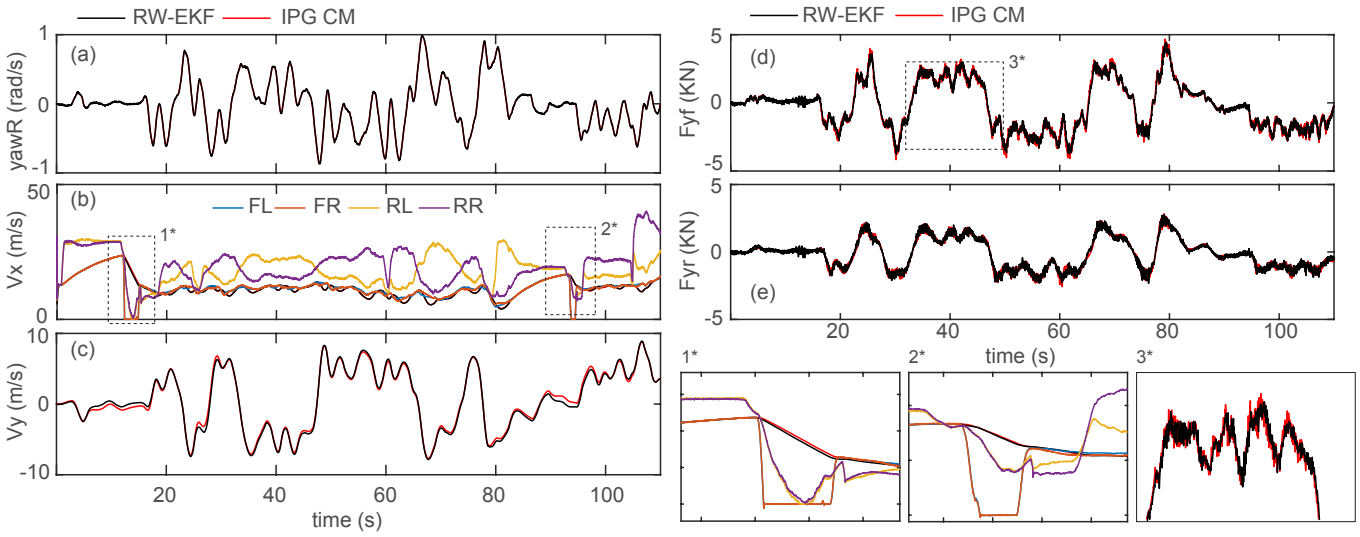

Fig. 12. Test (#2), Limit drifting on gravel. (a) Yaw rate, (b) Longitudinal velocity, (c) lateral velocity, (d) Front axle lateral force, (e) Rear axle lateral force.

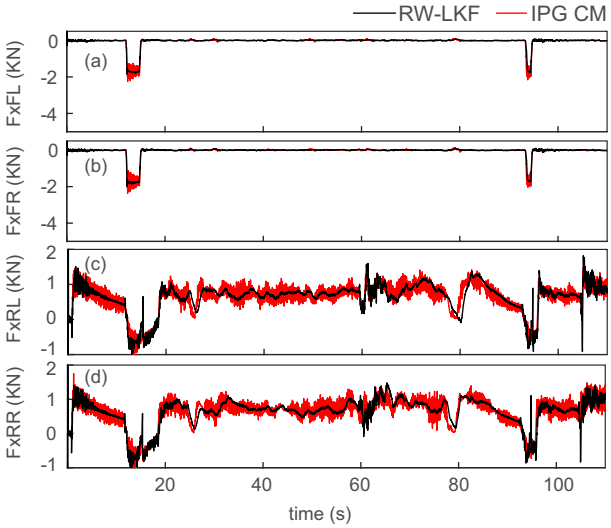

Fig. 13. Test (#2). Tyre longitudinal forces estimated by the RW-LKF.

TABLE IV
NRMSE OF THE MOTION STATES AND LATERAL FORCES.

Test	$e_{\dot{\psi}}$	e_{v_x}	e_{v_y}	e_{Fyf}	e_{Fyr}
#1	0.90	0.54	2.46	4.03	6.16
#2	0.94	1.16	3.83	4.03	5.64
#3	0.79	1.72	5.43	6.25	6.86
#4	1.92	1.52	5.81	7.38	7.44

or direct measurement of the "true" longitudinal velocity were assumed in the works cited previously. The proposed structure not only achieves similar performance levels but also eliminates these assumptions. Regarding the longitudinal force errors, values below the 10% error band are seen in the majority of the manoeuvres. Values exceeding this band are noticed occasionally when the longitudinal forces are reduced (e.g. non-driven wheels during power-slide). As was seen previously, the estimation of the vehicle motion states is very accurate in spite of these errors.

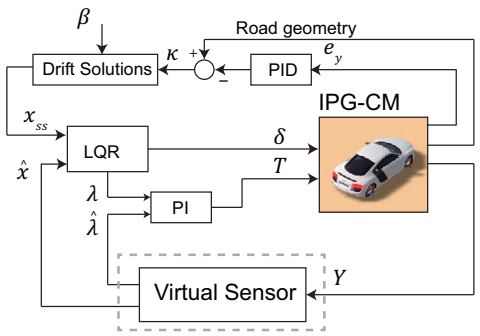

Fig. 14. Drift Controller Architecture.

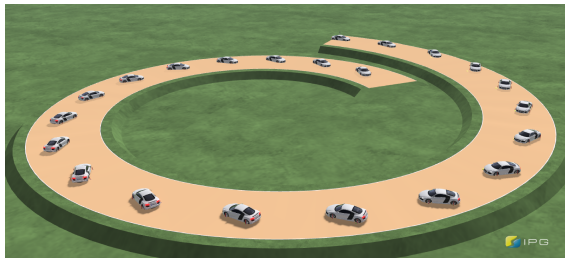

Fig. 15. Test (#4). Drift on clothoid. $R_{ini} = 50m$, $R_{final} = 25m$.

TABLE V
NRMSE OF THE ESTIMATED LONGITUDINAL FORCES.

Test	e_{Fxfl}	e_{Fxfr}	e_{Fxrl}	e_{Fxrr}
#1	9.19	9.33	8.98	7.68
#2	2.45	2.34	11.73	10.12
#3	9.50	2.98	8.08	6.55
#4	18.93	24.31	4.97	7.21

Remark: In Sections IV-A2 and IV-B2 the proposed observer was integrated into a conventional Yaw Stability Control (YSC) system and an Autonomous Drift Control (ADC) sys-

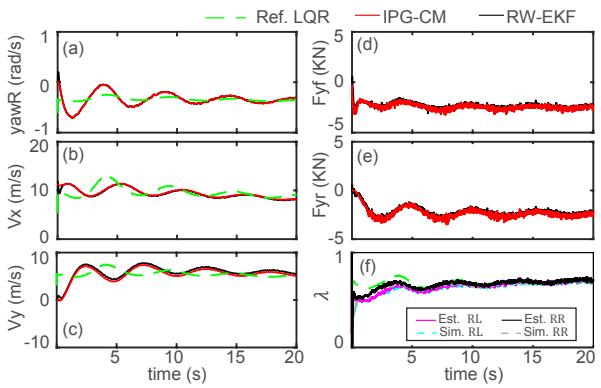

Fig. 16. Test (#4). Clothoid autonomous drift control. (a) Yaw rate, (b) Longitudinal velocity, (c) lateral velocity, (d) Front axle lateral forces, (e) Rear axle lateral forces and (f) rear longitudinal slips.

tem. The controllers performed with the embedded observers, restricting the maximum body slip in the case of the YSC and stabilising the vehicle around large body slips in the case of the ADC. Additional simulations (omitted here due to space limitations) were performed for different steering amplitudes (Sine with Dwell, YSC) and different clothoid geometries (ADC), and similar performance levels were seen. Despite further robustness analyses are still to be performed, these results indicate that the error levels obtained with the proposed virtual sensor are acceptable and do not compromise the controller actuation and subsequently the vehicle safety.

C. Road friction recognition

The trim drifting conditions are highly dependent on the road friction characteristics [1], [2]. Despite these equilibrium solutions can be computed offline for a set of surfaces and stored in Look-Up tables, a road friction recognition module is still required to determine whether the vehicle is being driven on a particular surface. As was seen in Section IV-A, a pattern recognition module relying exclusively on the road grip potential ([26], [22]) might be unable to perform this task robustly, as the grip scaling approach proposed in [17] is not suitable for off-road surfaces due to the severe distortion of the force versus slip curve. Instead, a more sophisticated feature vector including information such as the evolution of the cornering stiffness along the axle lateral slip might be necessary. An open-loop cornering stiffness reconstruction approach was proposed in [20] to compute this information offline. In this work, an online estimation strategy based on an ANFIS model is suggested. Specifically, the ANFIS model is adapted in real time to match the real friction characteristics, Section II-C1. The tests depicted in Fig. 17 were performed to verify this statement. In total, 4 sinusoidal manoeuvres were executed manually at a constant speed on different surfaces. In cases (1), (2), and (3), the ANFIS model is initialized as an empty model and driven over asphalt ($\mu_{\max} = 1$,$\mu_{\max} = 0.6$) and gravel-like ($\mu_{\max} = 0.6$) surfaces. An experimentally validated vehicle model used in previous works was employed during these tests [26]. Asphalt surfaces were simulated using an experimentally validated MF 6.1 Tyre model [26], while the gravel surface was modelled using the isotropic MF tyre model used in previous sections. During the first seconds of the tests, the adaptation algorithm described in Section II-C1 stores the information provided by the RW-EKF. Once enough information is gathered, the ANFIS model is trained and updated. As can be seen in Fig. 17, the ANFIS model adapts remarkably well to the road friction characteristics in high-mu asphalt, low-mu asphalt, and gravel-like surfaces. An additional test is depicted at the bottom of the figure, case (4), where the ANFIS model obtained in the gravel test is reused in high-mu asphalt conditions. The ANFIS model re-adapts quickly to the new road friction characteristics and provides accurate estimates after $t \approx 32s$, demonstrating the suitability of the ANFIS adaptation approach to tracking mu-varying conditions.

V. Experimental Validation

The proposed design was validated experimentally in Slalom and Fishhook tests using a Hatchback (Peugeot 308sw, Fig. 19) and a Luxury-SUV vehicle. The hatchback vehicle was instrumented with Kistler Roadyn S625 wheel force transducers and a Correvit S-400 sensor placed at the spare wheel location, between the rear axle and the rear bumper. A similar experimental setup was employed in the Luxury-SUV vehicle, but this time the vehicle slip was measured using inertial units attached to the rear wheels instead of an optical sensor. Additional details regarding the instrumentation of the latter vehicle are omitted due to confidentiality. The yaw rate, steering wheel angle, lateral acceleration, and longitudinal velocity signals were acquired directly from the CAN bus of both vehicles. The vehicle mass and centre of gravity location were obtained from tyre normal force measurements. A linear steering ratio coefficient was employed to calculate the angle steered by the front wheels, and the yaw inertia was computed from the vehicle mass using a radius of gyration approach ($I_z \approx m r_{gyr}^2$), where r_{gyr}^2 was set to 1.4 based on the compact-class vehicle data from the *IPG-CarMaker* library, and the same value was maintained for the Hatchback and SUV vehicles for simplicity. Overall, variations of the yaw inertia around the reference value had a small influence on the final results. Further investigations to study the robustness of the proposed approach to parameter uncertainties will be explored in the future. The manoeuvres were carried out on a proving ground (UTAC-CERAM, France and IDIADA, Spain) to avoid integrity issues on the experimental equipment. Moreover, the analysis was restricted to high-mu surfaces in this initial evaluation and the validation of the vehicle planar dynamics module under aggressive lateral dynamics was pursued. Due to limitations on the number of signals available, the longitudinal forces required by the vehicle planar dynamics block were provided directly by the wheel force transducers. Authors envisage that the results obtained in this work will motivate the execution of additional testing activities on loose surfaces to validate the complete structure proposed in this work in a wider range of driving events (with a special focus on limit drifting).

The results corresponding to the Fishhook test (limit A_y - 50kph) performed with the Luxury-SUV vehicle are depicted

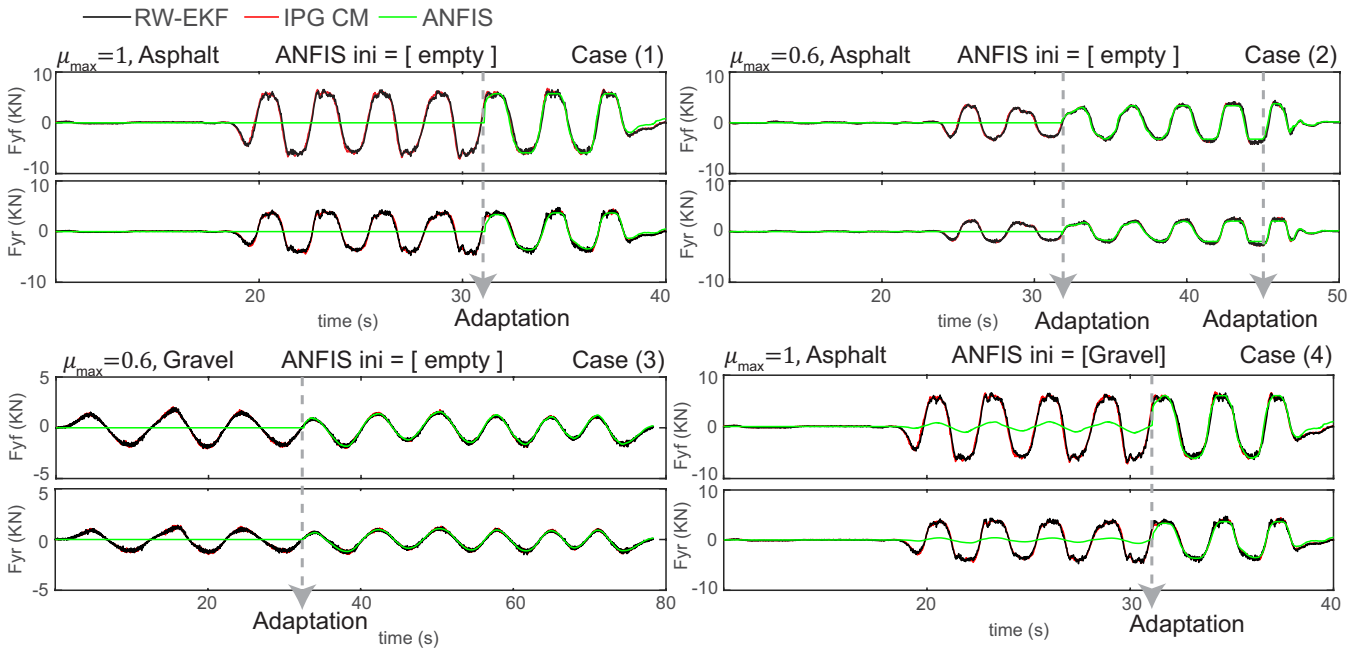

Fig. 17. Evaluation of the proposed ANFIS model for real-time road friction characterisation.

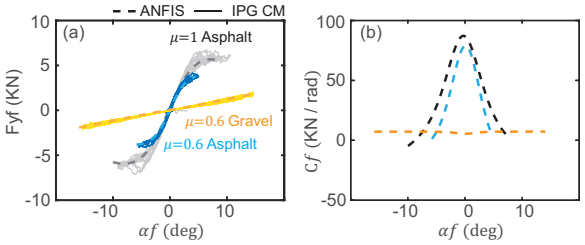

Fig. 18. Road friction characterisation with ANFIS. (a) Front axle lateral force, (b) Front axle cornering stiffness (C_f) versus lateral slip curve.

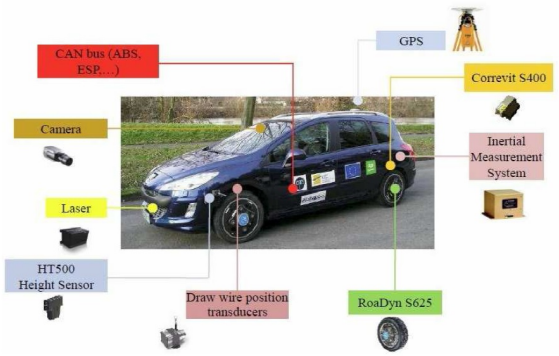

Fig. 19. Peugeot 308sw experimental testbed developed at Universitè de Technologie de Compiégne.

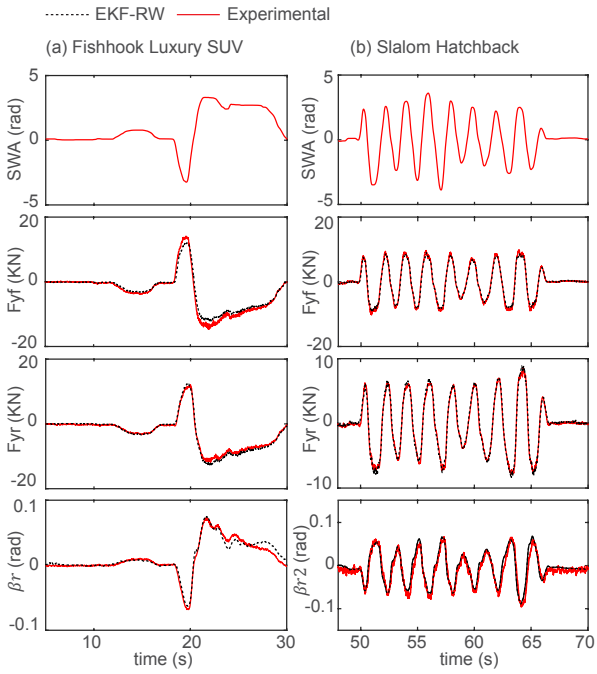

Fig. 20. (a) Experimental Fishhook test, IDIADA (Spain), luxury-SUV vehicle, and (b) Experimental Slalom test, UTAC-CERAM (France), Hatchback vehicle.

in Fig. 20-a. The estimated vehicle body slip was translated from the centre of gravity to the rear axle and compared to the average rear wheel slips measured with the inertial units, denoted as (β_r). Overall, the axle lateral forces and the rear axle slip are estimated accurately, being the $NRMS$ errors 6.84% and 4.59% for the front and rear lateral forces, and 7.06% for the rear axle slip. The results corresponding to the slalom test (limit A_y - 60kph) performed with the Hatchback vehicle are depicted in Fig. 20-b. The vehicle body slip measured at the spare wheel location (β_{r2}) has been represented unaltered, and the estimated body slip has been

translated to this position using the rest of estimated states. In this case, the $NRMS$ errors of the front and rear lateral forces are 6.57% and 4.91% respectively, and the β_{r2} error is slightly higher than in the Luxury-SUV vehicle, specifically 11.27%. Such mismatch between estimated and measured slip might be influenced by the noise level seen on the optical sensor. Despite this, errors keep close to the values found in other works where tyre model-based [13] or tyre model-less [11] approaches are validated experimentally. Moreover, it must be mentioned that acceptable results have been achieved with a minimum tuning effort between vehicles and employing inexpensive signals already available in the CAN bus, rather than using high-accuracy inertial measurements from expensive equipment, [20].

VI. Conclusions

A. Relevant Achievements

In this paper, a robust tyre-model-less virtual sensor to estimate the vehicle planar motion states and the tyre forces using exclusively standard sensor signals available on the CAN bus of modern vehicles has been presented. A novel modular filter architecture composed of Stochastic Kalman Filters has been proposed and the advantages of the proposed observer design with respect to previous approaches found in the literature have been evidenced by means of simulations on loose surfaces and inclined roads. Moreover, for the first time, the suitability of a vehicle dynamics state estimator for vehicle agile manoeuvring applications (e.g. drifting) has been evaluated. A virtual testing environment has been employed in *IPG-CarMaker®* for this purpose using a driver-in-the-loop setup. In addition to the verification of the virtual sensor on manual drifting manoeuvres, the proposed design has been embedded into an active drift controller formed by a gain-scheduled Linear Quadratic Regulator and autonomous drift stabilisation has been achieved for the first time using only readily-available measurements. In order to minimise the influence of the road friction uncertainties on the drift controller and facilitate the selection of the appropriate trim drifting conditions, the suitability of an ANFIS model to capture the road friction characteristics (axle lateral force versus axle lateral slip) has been evaluated. The adaptation algorithm proposed in this paper has been simulated under different road friction conditions and the ability of the ANFIS model to approximate the real friction characteristics has been verified. Finally, the vehicle planar dynamics block of the proposed structure has been validated experimentally under Slalom and Fishhook manoeuvres performed with Hatchback and Luxury-SUV vehicles respectively.

B. Current limitations and Future Research Steps

In the opinion of the authors, the major drawback of the proposed approach is that an immediate estimation of the road friction characteristics is not possible with the ANFIS model. Instead, an excitation period in which the data is gathered is required prior to the ANFIS adaptation. On the other hand, as was demonstrated in Section IV-A, the proposed approach does not fail on loose surfaces, as grip scaling-based approaches relying on a tyre model characterised on rigid surfaces are expected to do. During the next research steps, the adoption of a combined grip-identification scheme (as suggested in [47]), taking advantage of the vehicle longitudinal dynamics and tyre self-alignment torque measurements, will be investigated to reduce the excitation levels and time required to identify the friction characteristics.

To conclude, authors envisage that the proposed tyre-model-less structure can have a potential impact on vehicle controller development, lessening the considerable effort required to parameterize a tyre model in a wide range of firms and during extreme sliding conditions.

Acknowledgment

This project is part of the Interdisciplinary Training Network in Multi-Actuated Ground Vehicles (ITEAM) European program and has received funding from the European Unions Horizon 2020 research and innovation program under the Marie Sklodowska-Curie grant agreement No 675999. The authors want to thank Mr Jan Prins and Mr Mateo Gladstone, Jaguar Land Rover, Gaydon, United Kingdom, for their contribution to this work. M. E. Fitzpatrick is grateful for funding from the Lloyds Register Foundation, a charitable foundation helping to protect life and property by supporting engineering-related education, public engagement and the application of research.

References

[1] E. Velenis, D. Katzourakis, E. Frazzoli, P. Tsiotras, and R. Happee, "Steady-state drifting stabilization of rwd vehicles," *Control Engineering Practice*, vol. 19, no. 11, pp. 1363–1376, 2011.

[2] M. Acosta, S. Kanarachos, and M. Fitzpatrick, "A hybrid hierarchical rally driver model for autonomous vehicle agile maneuvering on loose surfaces." in *International Conference on Informatics in Control, Automation and Robotics.*, 2017.

[3] I. Chakraborty, P.Tsiotras, and J. Lu, "Vehicle posture control through aggressive maneuvering for mitigation of t-bone collision." in *IEEE Conference on Decision and Control*, 2011.

[4] D. Tavernini, M. Massaro, E. Velenis, D. Katzourakis, and R. Lot, "Minimum time cornering: the effect of road surface and car transmission layout," *Vehicle System Dynamics: International Journal of Vehicle Mechanics and Mobility*, vol. 51, no. 10, pp. 1533–1547, 2013.

[5] K. Nam, H. Fujimoto, and Y. Hori, "Estimation of sideslip and roll angles of electric vehicles using lateral force sensors through rls and kalman filter approaches," *IEEE Transactions on Industrial Electronics*, vol. 60, pp. 988–1000, 2013.

[6] A. Tuononen, "Vehicle lateral state estimation based on measured tyre forces." *Sensors.*, vol. 9, pp. 8761–8775, 2009.

[7] J. Edelmann, M. Gobbi, G. Mastinu, M. Ploechl, and G. Previati, "Friction estimation at tyre-ground contact," *SAE International Journal of Passenger Cars - Mechanical Systems.*, 2015.

[8] M. Acosta, S. Kanarachos, and M. Blundell, "Virtual tyre force sensors: A review on tyre model-based and tyre model-less state estimation techniques." *Proceedings of the Institution of Mechanical Engineers, Part D: Journal of Automobile Engineering.*, vol. In press, 2017.

[9] T. R. Botha, P. Els, B. Jacobson, and A. Albinsson, "Vehicle motion measurements using front facing camera and digital image correlation," in *ASME International Design Engineering Technical Conferences and Computers and Information in Engineering Conference.*, 2016.

[10] M. Hrgetic, J. Deur, D. Pavkovic, and P. Barber, "Adaptive ekf-based estimator of sideslip angle using fusion of inertial sensors and gps," *SAE International Journal of Passenger Cars - Mechanical Systems*, vol. 4, no. 1, pp. 700–712, 2011.

[11] E. Hashemi, M. Prani, A. Khajepour, A. Kasaiezadeh, S. Chen, and B. Litkouhi, "Corner-based estimation of tire forces and vehicle velocities robust to road conditions." *Control Engineering Practice.*, vol. 61, no. 2017, pp. 28–40, 2017.

[12] W. Cho, J. Yoon, S. Yim, B. Koo, and K. Yi, "Estimation of tire forces for application to vehicle stability control," *IEEE Transactions on Vehicular Technology*, vol. 59, no. 2, pp. 638–649, 2010.
[13] M. Doumiati, A. Charara, A. Victorino, and D. Lechner, *Vehicle Dynamics Estimation using Kalman Filtering*. Wiley-ISTE, 2012.
[14] S. Antonov, A. Fehn, and A. Kugi, "Unscented Kalman filter for vehicle state estimation," *Vehicle System Dynamics*, vol. 49, no. 9, pp. 1497–1520, 2011.
[15] M. Wilkin, W. Manning, D. Crolla, and M. Levesley, "Use of an extended kalman filter as a robust tire force estimator," *Vehicle Systems Dynamics*, vol. 44, no. sup1, pp. 50–59, 2006.
[16] H. Rui, E. Jimenez, D. Savitski, C. Sandu, and I. V., "Investigating the parameterization of dugoff tire model using experimental tire-ice data." *SAE International Journal of Passenger Cars - Mechanical Systems.*, vol. 10, no. 2016, 2016.
[17] H. Pacejka, *Tire and Vehicle Dynamics*. Butterworth-Heinemann, 2012.
[18] C. Liang, R. Allen, J. Rosenthal, and J. Chrstos, "Tire modeling for off-road vehicle simulation," *SAE Technical Papers*, 2004.
[19] K. Berntorp, B. Olofsson, K. Lundahl, and L. Nielsen, "Models and methodology for optimal trajectory generation in safety-critical road-vehicle manoeuvres," *Vehicle System Dynamics: International Journal of Vehicle Mechanics and Mobility*, vol. 52, pp. 1304–1332, 2014.
[20] M. Hrgetic, J. Deur, V. Ivanovic, and E. Tseng, "Vehicle sideslip angle ekf estimator based on nonlinear vehicle dynamics model and stochastic tire forces modeling," *SAE International Journal of Passenger Cars - Mechanical Systems*, vol. 2014, 2014.
[21] L. Ray, "Nonlinear state and tire force estimation for advanced vehicle control," *IEEE Transactions on Control Systems Technology*, vol. 3, no. 1, pp. 117–124, 1995.
[22] L. R. Ray, "Nonlinear tire force estimation and road friction identification: Simulation and experiments." *Pergamon*, vol. 33, pp. 1819–1833, 1997.
[23] P. Luque, D. Mantaras, E. Fidalgo, J. Alvarez, P. Riva, P. Giron, D. Compadre, and J. Ferran, "Tyre-road grip coefficient assessment - part ii: online estimation using instrumented vehicle, extended kalman filter, and neural network," *Vehicle Systems Dynamics: International Journal of Vehicle Mechanics and Mobility*, vol. 51, no. 12, pp. 1872–1893, 2013.
[24] C. Nuthong, *Estimation of tire-road friction forces using extended and unscented kalman filtering for advanced vehicle control, PhD Thesis*. Universitat der Bundeswehr Munchen, Germany, 2009.
[25] G. Baffet, A. Charara, and D. Lechner, "Estimation of vehicle sideslip, tire forces and wheel cornering stiffness," *Control Engineering Practice*, vol. 17, pp. 1255–1264, 2009.
[26] M. Acosta and S. Kanarachos, "Tire force estimation and road grip recognition using extended kalman filter, neural networks and recursive least squares," *Neural Computing and Applications, Springer*, vol. 2017, pp. 1–21, 2017.
[27] M. Acosta, S. Kanarachos, and M. Fitzpatrick, "A virtual sensor for integral tire force estimation using tire model-less approaches and adaptive unscented kalman filter." in *International Conference on Informatics in Control, Automation and Robotics.*, 2017.
[28] A. Albinsson, F. Bruzelius, M. Jonasson, and B. Jacobson, "Tire force estimation utilizing wheel torque measurements and validation in simulations and experiments," in *Proceedings of the 12th International Symposium on Advanced Vehicle Control*, 2014.
[29] M. Acosta, A. Alatorre, S. Kanarachos, A. Victorino, and A. Charara, "Estimation of tire forces, road grade, and road bank angle using tire model-less approaches and fuzzy logic." in *World Congress of the International Federation of Automatic Control.*, 2017.
[30] U. Kiencke and L. Nielsen, *Automotive Control Systems: For engine, driveline, and Vehicle*. Springer, 2005.
[31] W. Klier, A. Reim, and D. Stapel, "Robust estimation of vehicle sideslip angle – an approach w/o vehicle and tire models," in *Proceedings of the SAE World Congress*, 2008.
[32] H. Hamann, J. Hedrick, S. Rhode, and F. Gauterin, "Tire force estimation for a passenger vehicle with the unscented kalman filter," in *IEEE Intelligent Vehicles Symposium*, 2014.
[33] J. Jang, "Anfis: Adaptive-network-based fuzzy inference system." *IEEE Transactions on Systems, Man, and Cybernetics.*, vol. 23, pp. 665–685, 1993.
[34] P. Young, *Recursive Estimation and Time-Series Analysis*. Springer, 2011.
[35] RaceLogic, *RLVBIMU04 Inertial Motion Unit Technical datasheet*. Racelogic, 2015.
[36] W. Wang, J. Xi, and X. Li, "Statistical pattern recognition for driving styles based on bayesian probability and kernel density estimation." *International Journal of Automotive Technology*, 2016. [Online]. Available: http://arxiv.org/abs/1606.01284
[37] D. Kasper, G. Weidl, T. Dang, G. Breuel, A. Tamke, A. Wedel, and W. Rosenstiel, "Object-oriented bayesian networks for detection of lane change maneuvers." *Intelligent Transportation Magazine.*, vol. 4, pp. 1–10, 2012.
[38] Y. Zhang, W. Lin, and Y. Chi, "A pattern-recognition approach for driving skill characterization." *IEEE Transactions on Intelligent Transportation Systems.*, vol. 11, pp. 905–916, 2010.
[39] B. Higgs and M. Abbas, "Segmentation and clustering of car-following behavior: recognition of driving patterns." *IEEE Transactions on Intelligent Transportation Systems.*, vol. 16, pp. 81–90, 2015.
[40] M. Acosta, S. Kanarachos, and M. E. Fitzpatrick, "Accurate virtual sensing of vertical tire forces for enhanced handling dynamics." in *43rd Annual Conference of the IEEE Industrial Electronics Society, IECON.*, 2017.
[41] M. Sayers, *Dynamic Terrain Inputs to Predict Structural Integrity of Ground Vehicles*. The University of Michigan Transportation Research Institute, 1998.
[42] I. O. for Standardization, *BS ISO 8608:2016 Mechanical vibration - Road surface profiles - Reporting of measured data*. BSI Standards publication, 2016.
[43] J. Rauh, *A unified approach to represent 3D road data in tyre simulation*. Daimler AG, 2008.
[44] R. Rajamani, *Vehicle Dynamics and Control*. Springer, 2012.
[45] M. Acosta, "Research on multi-actuated agile electric vehicles: A drift-based approach to last-moment accident avoidance manoeuvres on loose surfaces, phd progress report," *Coventry University, DOI: 10.13140/RG.2.2.14132.96640*, 2017.
[46] C. Ifedi, *A High Torque Density, Direct Drive In-wheel Motor for Electric Vehicles, Ph.D Thesis*. Newcastle University, 2013.
[47] C. Ahn, *Robust Estimation of road friction Coefficient, PhD Thesis*. University of Michigan, USA, 2011.

Manuel Acosta gained his Masters degree in Machinery Design and Transportation in Carlos III University (Madrid, 2014). In the same year, he enrolled as Data Analyst and Scrutineering engineer in the European Championship International GT Open, as part of the motorsport Start-up Automotiva. In 2015 he started working for the Vehicle Dynamics Department of IDIADA Automotive Technology (Barcelona, Spain). He is currently a Marie Curie Fellow at Coventry University (UK). His research interests include vehicle state estimation and chassis control systems.

Stratis Kanarachos received the Diploma in Mechanical Engineering from the National Technical University of Athens in 2001 and the Ph.D. degree from the National Technical University of Athens in 2004. He has worked at the Frederick University with the Mechanical Engineering Department, Cyprus (2005-2012), at TNO with the Integrated Vehicle Safety Department, Netherlands (2012-2014) and at the Technical University of Eindhoven (2014). He is currently a Reader at Coventry University with the School of Engineering, Environment and Computing. His research interests include modelling using Deep Neural Networks, Intelligent Systems, Neural Networks and Optimization.

Professor Michael E. Fitzpatrick is the Executive Dean of the Faculty of Engineering, Environment and Computing at Coventry University, and holds the Lloyds Register Foundation Chair of Materials Fabrication and Engineering. His research centres around the application of advanced experimental methods to materials engineering applications, particularly in the nuclear power and aerospace industries. He has published over 150 research papers. His recent interests include the study of laser shock peening for life enhancement of aerospace and marine structures and the development of novel structural concepts such as bonded crack retarders for improving airframe structural integrity.